



HAL
open science

Enhanced organic degradation and biogas production of domestic wastewater at psychrophilic temperature through submerged granular anaerobic membrane bioreactor for energy-positive treatment

Lucie Sanchez, Morgane Carrier, Jim Cartier, Christophe Charmette, Marc Heran, Geoffroy Lesage, Jean-Philippe J.-P. Steyer

► To cite this version:

Lucie Sanchez, Morgane Carrier, Jim Cartier, Christophe Charmette, Marc Heran, et al.. Enhanced organic degradation and biogas production of domestic wastewater at psychrophilic temperature through submerged granular anaerobic membrane bioreactor for energy-positive treatment. *Bioresource Technology*, 2022, 353, pp.127145. 10.1016/j.biortech.2022.127145 . hal-03709141

HAL Id: hal-03709141

<https://hal.inrae.fr/hal-03709141>

Submitted on 9 Oct 2023

HAL is a multi-disciplinary open access archive for the deposit and dissemination of scientific research documents, whether they are published or not. The documents may come from teaching and research institutions in France or abroad, or from public or private research centers.

L'archive ouverte pluridisciplinaire **HAL**, est destinée au dépôt et à la diffusion de documents scientifiques de niveau recherche, publiés ou non, émanant des établissements d'enseignement et de recherche français ou étrangers, des laboratoires publics ou privés.

1 **Enhanced organic degradation and biogas production of**
2 **domestic wastewater at psychrophilic temperature through**
3 **submerged granular anaerobic membrane bioreactor for**
4 **energy-positive treatment**

5 Lucie Sanchez^a, Morgane Carrier^a, Jim Cartier^a, Christophe Charmette^a, Marc Heran^a,
6 Jean-Philippe Steyer^b, Geoffroy Lesage^a

7 ^a Institut Européen des Membranes (IEM), Université de Montpellier, CNRS, ENSCM,
8 Montpellier, France

9 ^b INRAE, Univ Montpellier, LBE, Narbonne, France

10 **ABSTRACT**

11 This study deals with the conversion of organic matter into methane at ambient
12 temperature, during anaerobic digestion of domestic wastewater combined with a submerged
13 ultrafiltration membrane with no gas-sparging. A one-stage submerged granular anaerobic
14 membrane bioreactor (G-AnMBR) and a control anaerobic digester (UASB type) were
15 operated during four months, after 500 days of biomass acclimatization to psychrophilic and
16 low loading rate conditions. Membrane barrier led to the retention of biomass, suspended
17 solids and dissolved and colloidal organic matter which greatly enhanced total COD (tCOD)
18 removal (92.3%) and COD to methane conversion (84.7% of tCOD converted into dissolved
19 and gaseous CH₄). G-AnMBR overcame the usual long start-up period and led to a higher
20 sludge heterogeneity, without altering the granular biomass activity. The feasibility of the G-
21 AnMBR without gas-sparging was also assessed and the net positive energy balance was
22 estimated around +0.58 kWh.m⁻³.

23 **KEYWORDS**

24 ultrafiltration; anaerobic digestion; granular biomass; low-strength wastewater; energy
25 recovery.

26 **1. Introduction**

27 For the last decade, large attention has been given to establish a balance between human
28 well-being and environment preservation. In this way, intensive resource use is switching into
29 a circular economy approach, based on the reuse and recycling of resources. For those
30 reasons, wastewater is not only considered as an alternative source of water but also as a
31 source of nutrients, minerals and energy (Batstone and Viridis, 2014). In this sustainable
32 development context, anaerobic digestion (AD) presents many advantages over conventional
33 activated sludge (CAS) processes for domestic wastewater treatment (DWWT) since (i) it
34 does not require aeration, which decreases energy-demand and associated costs, (ii) it
35 produces a smaller amount of sludge, begetting less sludge processing and disposal
36 difficulties and costs, and (iii) it converts organic matter into energy in the form of methane
37 (van Lier et al., 2008). Recent studies have evaluated a world domestic wastewater production
38 of $359.10^9 \text{ m}^3 \cdot \text{year}^{-1}$ (Jones et al., 2021) with a chemical oxygen demand (COD) concentration
39 between 210 and 740 $\text{mgCOD} \cdot \text{L}^{-1}$ (Srinivasa Raghavan et al., 2017). Based on the theoretical
40 conversion rate of $0.35 \text{ m}^3 \cdot \text{CH}_4 \cdot \text{kgCOD}^{-1}$ and the calorific energy of methane of $35.9 \text{ kJ} \cdot \text{L} \cdot$
41 CH_4^{-1} , it appears that 263-903 $\text{TWh} \cdot \text{year}^{-1}$ of energy could be recoverable from wastewater
42 through AD, that means up to a third of the electricity consumed by the European Union. It
43 highlights the high bioenergy potential of anaerobic domestic wastewater treatment as an
44 alternative through fossil consumption and an ease on energy insecurity (Chen et al., 2016).

45 However, the feasibility of the dominant anaerobic technologies (i.e. upflow anaerobic
46 sludge blanket (UASB) and expended granular sludge bed (EGSB)) for domestic wastewater
47 is challenged by low influent substrate concentration, huge wastewater quantities and

48 psychrophilic temperature (≤ 25 °C) (Maaz et al., 2019; Vinardell et al., 2020). Thus, even if
49 the UASB are applied to domestic wastewater in some tropical countries (i.e. Brazil, India,
50 Colombia), UASB treatment plants still exhibit substandard effluent quality discharge and
51 poor biogas production (Chernicharo et al., 2015; Srinivasa Raghavan et al., 2017; Kong et
52 al., 2021b). Anaerobic membrane bioreactor (AnMBR) has been found to overcome UASB
53 weakness since it enables to operate at high sludge retention times (SRT) and short hydraulic
54 retention times (HRT). Therefore, even at high volumetric flow rates, ultrafiltration
55 membrane rejection ensures the growth of slow anaerobic communities and, as a result,
56 improves the conversion of organic matter into methane energy content (Ji et al., 2021;
57 Robles et al., 2018). Plus, the membrane unit performs pathogens rejection and could improve
58 organic micropollutants removal (Robles et al., 2018). Since no nitrogen and phosphorus
59 degradation is expected from AD, the nutrients-rich effluent could be viewed as a valuable
60 product suitable for reuse applications (e.g. fertilizer, irrigation) (Maaz et al., 2019). Thus,
61 AnMBR has the potential to produce a relevant effluent for water reuse while performing a
62 positive net energy balance (NEB) (Robles et al., 2018; Vinardell et al., 2020). Nevertheless,
63 dissolved methane and membrane fouling are key issues for full-scale implementation (Maaz
64 et al., 2019). The loss of energy, in the form of dissolved methane within the effluent, is a
65 well-known issue for anaerobic wastewater treatment at psychrophilic temperature, due to the
66 methane solubility increase with a decrease in temperature and the entrapment of biogas
67 inside the sludge bed. Typical dissolved methane concentration ranges between 10 and 25
68 mg-CH₄.L⁻¹ and up to 100% of the total produced methane could be lost in the effluent
69 (Sohaib et al., 2022). Fortunately, developing processes, such as degassing membrane, air
70 stripping oxidation and engineered methanotrophic community in photogranules, have proven
71 their ability to remove most of the dissolved methane which is attractive for energy recovery

72 and/or to prevent greenhouses gas (GHG) emissions (Robles et al., 2018; Safitri et al., 2021;
73 Sohaib et al., 2022).

74 As for now, the major constraint to achieve energy-positive AnMBR is membrane
75 fouling (Maaz et al., 2019). Submerged membrane configuration presents the advantages to be
76 less energy-consuming for suction and more compact (Liao et al., 2006), nonetheless, it
77 implies that gas-sparging is the easiest way to mitigate membrane fouling. Studies based on
78 AnMBR energy demand stated that more than 70% of the energy consumption owed to gas-
79 sparging for fouling control (Batstone and Viridis, 2014; Smith et al., 2014). To cut the high
80 operational cost, several research have been undertaken to understand, limit and control
81 membrane fouling (Robles et al., 2018).

82 Granular anaerobic membrane bioreactor (G-AnMBR), a hybrid biotechnology that
83 incorporates AnMBR and granular biomass, has raised attention as a sustainable AD process
84 (Vinardell et al., 2020). Granular sludge presents a great advantage over flocculent sludge for
85 its (i) high settling capacity, (ii) well-balanced bacteria consortia, (iii) compact and dense
86 biomass structure and (iv) high-strength to loading rates and toxics shocks (van Lier et al.,
87 2008). As a result, previous studies stated that granular biomass technology increases
88 biological removal efficiencies, methane production yield and membrane mitigation (Deng et
89 al., 2020; Iorhemen et al., 2017). Therefore, the G-AnMBR configuration could be a way to
90 work without an energy-intensive gas-sparging fouling control strategy and could lead to a
91 process where the energy recovery overcomes the energy consumption of the system (Smith
92 et al., 2014).

93 The novelty of this research lies in the unusual G-AnMBR configuration that combines
94 a granular biomass and a membrane submerged directly inside the sludge bed, without gas-
95 sparging for fouling control. Hence, the objective of this paper is two-fold. First, to evaluate

96 and understand the impact of a submerged membrane inside a granular anaerobic digester (i.e.
97 one-stage reactor), focusing on the treatment performances, biogas production and granular
98 biomass behavior. Second, to study the feasibility of an efficient and positive-energy DWWT
99 through G-AnMBR at 25°C, without gas-sparging for fouling mitigation. Therefore, a
100 submerged G-AnMBR and an UASB, as a control reactor, have been continuously operated
101 during four months with the same operating conditions.

102 **2. Materials and methods**

103 **2.1 Inoculum and wastewater composition**

104 The seed granular sludge was taken from a full-scale UASB, treating the sewage from a
105 manufacturer of recycled paper (Saica Paper Champblain-Laveyron, France), at mesophilic
106 temperature (35-38°C) with an organic loading rate (OLR) of 18 kgCOD.m⁻³.d⁻¹. The granular
107 biomass was gradually acclimatized to ambient temperature (25°C) and low-strength synthetic
108 wastewater during a period of 500 days (see supplementary material). The lab-scale reactors
109 were then inoculated with the acclimatized anaerobic granular sludge at a concentration of 70
110 ± 9.7 and 66 ± 9.2 gTS/L for the UASB and G-AnMBR respectively. The influent
111 composition was adjusted from Layer et al. (2019) with a C:N:P ratio of 100:1:0.2 and a COD
112 concentration corresponding to low-strength wastewater (WW). This complex synthetic WW
113 was chosen for its capacity to lead to the development of granular sludge with the same
114 characteristics to those fed with raw WW (Layer et al., 2019). The synthetic WW was
115 prepared weekly and stored under mixing at 4°C. The influent was characterized by total
116 COD (tCOD) of 274 ± 76 mgCOD.L⁻¹, soluble COD (sCOD) of 224 ± 65 mgCOD.L⁻¹,
117 particulate COD (pCOD) of 50 ± 27 mgCOD.L⁻¹, dissolved organic carbon (DOC) of 98 ± 30
118 mgC.L⁻¹, volatile fatty acids (VFA) of 130 ± 32 mgCOD.L⁻¹, ammonia (NH₄⁺-N) of 3.8 ± 1.6
119 mgN.L⁻¹, nitrite (NO₂⁻-N) of 0.2 ± 0.1 mgN.L⁻¹, orthophosphate (PO₄³⁻-P) of 0.5 ± 0.2 mgP.L⁻¹

120 ¹, sulfate (SO_4^{2-}S) of $11.0 \pm 0.5 \text{ mgS.L}^{-1}$. pCOD and VFA represent about 20% and 50%
121 respectively of the influent tCOD.

122 **2.2 Experimental set-up and operating conditions**

123 Two granular anaerobic reactors, namely G-AnMBR and UASB (as a control reactor),
124 were continuously operated in parallel during 120 days. The two experimental lab-scale
125 reactors consisted of parallelepiped-shaped tanks with equal working volume of 6.2 L (see
126 supplementary material). The liquid level was automatically controlled by a vibronic point
127 level detector (Liquiphant FTL31, Endress+Hauser, Switzerland). The synthetic wastewater
128 was introduced at the bottom of each reactors and flowed upwards the granular sludge bed. At
129 the top of the two reactors, supernatant was pumped through a peristaltic pump (Watson
130 Marlow (WMFTG), UK) and recirculated at the lower part to bring additional turbulences and
131 homogenized the dissolved phase. The upflow liquid velocity (ULV) was set around 2 m.h^{-1} .
132 A polyethersulfone (PES) flat sheet membrane (Microdyn-Nadir®, Germany) with a nominal
133 pore size of $0.04 \mu\text{m}$ and a surface area of 0.34 m^2 was submerged at the center of the one-
134 stage G-AnMBR reactor. The permeate was obtained through a peristaltic pump (LeadFluid®,
135 China) and the net filtration flux was maintained at $1.45 \pm 0.35 \text{ L.m}^{-2}.\text{h}^{-1}$ (LMH). Only an
136 automatic intermittent suction cycle was performed to mitigate membrane fouling at a low
137 energy-demand. The operation cycle was as follows: (i) 8 min 15 s of filtration, (ii) 30 s of
138 initial relaxation, (iii) 45 s of backwash and (iv) 30 s of final relaxation. To get as close as
139 possible to the G-AnMBR configuration and its hydrodynamic pathway, the same membrane
140 module was immersed in the UASB tank but no permeate was suctioned through this
141 membrane. The UASB effluent was pumped through supernatant with the same operation
142 cycle as the G-AnMBR. As shown in Table 1, similar operating conditions were applied in
143 both reactors. The reactors were equipped with temperature sensor, pH and oxidation
144 reduction potential (ORP) probes (PCE Instruments, Deutschland). The physico-chemical

145 parameters were stable during the campaign and the very low redox (< -450 mV) values
146 confirm that anaerobic conditions were fulfilled. The reactor temperature was kept at around
147 25°C with a cryostat through a tubular heat exchanger. The hydraulic retention time (HRT)
148 and the OLR were maintained at 13 h and 0.5 kgCOD.m⁻³.d⁻¹. Pressure sensors were installed
149 to monitor atmospheric pressure (Patm), reactors headspace pressures and permeate pressure
150 to obtain the transmembrane pressure (ATM.ECO, Sensor Technik Sirmach (STS),
151 Switzerland). No sludge was intentionally purged except for the need of sampling.

152 **2.3 Analytical methods**

153 DOC was analyzed two days a week on sample pre-filtered at 0.22 µm by TOC analyzer
154 (TOC-V_{CSN}, Shimadzu Corporation, Japan). Mixed liquor suspended solids (MLSS) and
155 mixed liquor volatile suspended solids (MLVSS) were measured weekly in the UASB
156 effluent and G-AnMBR permeate according to Standard Methods (APHA et al., 1998). COD
157 concentrations were determined twice a week using pre-dosed photochemical test (Hach,
158 Germany, LKC 500, 314, 1414, 514) and UV-Vis spectrophotometer (DR3900, Hach,
159 Germany). sCOD was measured after sample filtration through 0.22 µm syringe filter. The
160 denominated tCOD and sCOD removal rates (tCOD_{removal} and sCOD_{removal} respectively) were
161 calculated as follow:

$$tCOD_{removal} = \frac{tCOD_{in} - tCOD_{out}}{tCOD_{in}} = \frac{COD_{removed}}{tCOD_{in}} \quad \text{Eq. 1}$$

$$sCOD_{removal} = \frac{tCOD_{in} - sCOD_{out}}{tCOD_{in}} \quad \text{Eq. 2}$$

162 where tCOD_{in} is the tCOD measured in the influent, tCOD_{out} is the tCOD of the effluent and
163 sCOD_{out} is the effluent sCOD concentration.

2.4 Three-dimensional fluorescence excitation-emission matrix (3DEEM)

Supernatant from G-AnMBR and effluents from both reactors were pre-filtered through 1.2 μm filter (Grade GF/C, Whatman, UK) and diluted 25 times to limit overlapping signals. The three-dimensional fluorescence excitation-emission matrix (3DEEM) was divided into four areas according to their respective fluorophores and the volume of fluorescence beneath each region were obtained according to Jacquin et al. (2017). The volume of fluorescence (in arbitrary unit per nm^2 (A.U/ nm^2)) gives a semi-quantitative information about the amount of fluorophores for each region.

2.5 Granular sludge characteristics

Total solids (TS) and Volatile solids (VS) were measured during reactor seeding according to Standard Methods (APHA et al., 1998). Sludge volume index after 10 minutes (SVI_{10}) and 30 minutes (SVI_{30}) were evaluated by dividing the volume of sludge bed (mL) by the initial sample volume (mL) and the TS concentration of the sample ($\text{gTS}\cdot\text{L}^{-1}$). The zeta potential of the sludge was measured by Litesizer 500 (Anton Paar, Spaar). The particle size distribution (PSD) of the granular sludge was performed by wet sieving following the method of Derlon et al. (2016) with standard sieves of 0.63 and 0.125 mm mesh sizes. Hence, the sludge was separated into three fractions based on the particle diameter (d_p) such as: (i) large granules with a d_p higher than 0.63 mm ($d_{p \geq 0.63}$), (ii) medium granules mixed with small granules with a d_p between 0.63 and 0.125 mm ($d_{p 0.125-0.63}$) and (iii) flocs for the sludge with a d_p less than 0.125 mm ($d_{p \leq 0.125}$). TS and VS of each fraction were measured. The proportion of each class of sludge was expressed as percentage of total sludge mass (Eq. 3). VS/TS ratio was calculated within the fractions.

$$\text{Mass fraction}_i (\%) = \frac{m_i}{\sum_1^3 m_i} \times 100 \quad \text{Eq. 3}$$

186 **2.6 Methane production**

187 Produced methane was measured in the gas and liquid phases. The gas phase flow rate
188 was continuously recorded by a volumetric flowmeter (MilliGas Counter, Ritter, Germany).
189 Biogas composition of the headspace was regularly analyzed by a gas chromatography system
190 (Clarus 400, Perkin Elmer, USA) coupled with a thermal conductivity detector at 150°C (GC-
191 TCD). Gas phase was collected through a quick gas connection (Swagelok, USA) into an
192 airtight system. 300 µL of the biogas was then sampled through a septum using a gastight
193 syringe (Hamilton Company, USA) and injected into GC-TCD. Methane concentration was
194 defined as the average of all measurements performed during the stable phase of operation.
195 Methane flow rate was converted in NL-CH₄.day⁻¹ by using the average temperature and the
196 atmospheric pressure (*P*_{atm}) of the day. Dissolved methane was quantified based on the
197 headspace method (Giménez et al., 2012; Souza et al., 2011). Vials equipped with a stirrer
198 (total volume (*V*_T) of 11.6 mL) were sealed with a septum cap and drained with helium during
199 10 min to avoid any presence of air. A known volume of effluent sample (*V*_L) was collected
200 using a gastight syringe (Hamilton Company, USA) and injected in sealed vials. Then, vials
201 were kept for stirring at 700 rpm and 25°C for 2h in order to reach gas/liquid equilibrium.
202 Once the equilibrium reached, the total pressure of the headspace (*P*_T) was recorded and the
203 biogas was analyzed through GC-TCD to determine the methane molar fraction (*y*_{CH₄}). The
204 dissolved methane concentration (*C*_{CH₄}^L) in the effluent was then calculated according to the
205 following expressions:

$$C_{CH_4}^L = \frac{C_{CH_4}^G \times (V_G + \frac{V_L}{H(T)})}{V_L} \quad \text{Eq. 4}$$

206 with

$$C_{CH_4}^G = \frac{y_{CH_4} \times P_T \times MM(CH_4)}{R \times T} \quad \text{Eq. 5}$$

207 where $C_{CH_4}^G$ is the CH_4 concentration in the gas phase ($mg.L^{-1}$), V_G is the volume of the gas
 208 phase (L), $MM(CH_4)$ is the molecular weight of methane ($16g.mol^{-1}$), R is the universal
 209 constant of gases ($0.082 atm.L.mol^{-1}.K^{-1}$), T is the temperature (K) and $H(T)$ is the
 210 dimensionless temperature-dependent Henry's constant for methane (Giménez et al., 2012).
 211 The saturation degree was calculated based on the theoretical value of methane dissolved in
 212 the liquid phase ($C_{CH_4}^{L*}$, in $mg.L^{-1}$) calculated according to the Henry's law thermodynamic in
 213 equilibrium with the gas phase as described in Eq. 6.

$$Saturation\ degree = \frac{C_{CH_4}^L}{C_{CH_4}^{L*}} = \frac{C_{CH_4}^L}{H(T) \cdot C_{CH_4}^G} \quad Eq. 6$$

214 **2.7 COD mass balance**

215 The COD mass balance was determined based on Eq. 7:

$$tCOD_{in} = tCOD_{out} + COD_{CH_4}^G + COD_{CH_4}^L + COD_{SO_4} + \Delta COD_{biomass} \quad Eq. 7$$

216 where $tCOD_{in}$ and $tCOD_{out}$ are the tCOD measured in the influent and effluent respectively,
 217 $COD_{CH_4}^G$ and $COD_{CH_4}^L$ correspond to the methane quantified in the gas and liquid phase
 218 respectively and converted in equivalent COD using the empirical relationship of $0,38 L-$
 219 $CH_4.gCOD^{-1}$ at $25^\circ C$. COD_{SO_4} is the theoretical COD used for sulfate reduction by sulfate-
 220 reducing bacteria (SRB) based on the experimental amount of sulfate removal measured and
 221 the theoretical value of $0.67 gCOD.gSO_4^{-1}$. The residual COD was considered as biomass
 222 conversion ($\Delta COD_{biomass}$) and used to calculate the sludge yield (Y_H) of granular biomass as
 223 follows :

$$Y_H = \frac{\Delta COD_{biomass}}{1.42 \cdot COD_{removed}}$$

224 where Y_H is in $\text{gVSS} \cdot \text{gCOD}_{\text{removed}}^{-1}$, $\Delta COD_{biomass}$ is in $\text{gCOD} \cdot \text{day}^{-1}$, $COD_{removed}$ is in
 225 $\text{gCOD}_{\text{removed}} \cdot \text{day}^{-1}$ and 1.42 is the COD to VSS ratio based on the biomass stoichiometry
 226 ($\text{C}_5\text{H}_7\text{O}_2\text{N}$) (van Lier et al., 2008).

227 **3. Results and discussion**

228 **3.1 AnMBR and UASB organic conversion and effluent quality**

229 **3.1.1 Organic matter removal**

230 Fig. 1 presents the tCOD and sCOD removal rate in the G-AnMBR and UASB reactors
 231 during the overall operation period. Table 2 gives complementary results of the average
 232 concentrations of tCOD, sCOD, DOC, MLSS and MLVSS measured in the outlets of both
 233 reactors. During the first month of the experiment, the UASB reactor had a very poor tCOD
 234 removal efficiency compared to the G-AnMBR reactor which was almost directly stable and
 235 efficient ($35.9 \pm 12.6\%$ and $81.6 \pm 3.8\%$ respectively (Table 2)). This difference is clearly due to
 236 the UF membrane separation that retains all particles and most of the dissolved and colloidal
 237 organic matter (DCOM) in the G-AnMBR whereas small granules, flocs and free-bacteria,
 238 just as some DCOM and intermediate degradation products, were washed-out within the
 239 supernatant of the UASB (Chen et al., 2017; Ozgun et al., 2015). This can be confirmed by
 240 the high amount of MLSS measured in the UASB effluent during the transient period (Table
 241 2) and the same concentration profiles followed by total COD and TSS. As a result, the
 242 removal rate for tCOD in the UASB showed an increasing trend until it achieved a steady-
 243 state after 31 days of operation. After the transient period, high organic removal efficiencies
 244 were carried out in both reactors, as describes in Table 2. Most notably, the G-AnMBR
 245 performed higher organic compounds removal ($92.3 \pm 4.1\%$ of tCOD, $90.0 \pm 5.4\%$ of sCOD

246 and $97.8 \pm 1.0\%$ of DOC) in comparison to the UASB ($79.2 \pm 8.5\%$, $80.7 \pm 7.3\%$ and
247 $86.5 \pm 9.1\%$ of tCOD, sCOD and DOC respectively). This result is well in line with previous
248 studies wherein 40-80% of the tCOD was removed by UASB reactors (Chernicharo et al.,
249 2015) and 71-98% by AnMBR at psychrophilic temperature (see supplementary material).
250 Hence, it appears that the G-AnMBR configuration without gas sparging permits the
251 degradation of organic compounds as high as gas-sparging ones.

252 Relevant differences in sCOD were observed between G-AnMBR supernatant
253 ($55.3 \pm 16.3 \text{ mgCOD.L}^{-1}$) and sCOD permeate ($17.4 \pm 4.3 \text{ mgCOD.L}^{-1}$) indicating that a part
254 of soluble compounds does not pass across the membrane. Hence, $16.4 \pm 4.7\%$ of the entering
255 sCOD is retained by the membrane barrier and/or removed by the biofilm. The average pore
256 size of the flat sheet membrane is $0.04 \mu\text{m}$ therefore a part of DCOM (i.e. proteins,
257 polysaccharides, humic aggregates) was expected to be retained by the membrane due to their
258 size. Mechanisms responsible of the retention of the soluble and colloidal matter can be either
259 related to physical phenomenon (i.e. size exclusion, adsorption, charge exclusion) as well as
260 microbial biofilm activity (Smith et al., 2013). Since no COD accumulation was observed in
261 the G-AnMBR supernatant, it can be reasonably assumed that the membrane provides a
262 physical barrier to slowly-biodegradable and non-settleable compounds (e.g. flocs, particles)
263 or by-products (e.g. products from polymers hydrolysis, proteins, SMP) which are later
264 biologically transformed thanks to a longer contact time between bulk sludge and organic
265 material (Gouveia et al., 2015; Ozgun et al., 2015) and thus, explains the enhanced G-
266 AnMBR performances on organic matter removal.

267 Table 3 and Fig. 2 provides complementary information about DCOM behavior inside
268 the anaerobic reactors. Comparing the total volume of fluorescence of the two effluents, it is
269 noticeable that more organics were removed in the G-AnMBR. On average 42.3% of the
270 fluorescent compounds present in the supernatant of the G-AnMBR did not pass through the

271 membrane. It can be seen from 3DEEM spectra (Fig. 2) and membrane retention rate (Table
272 3) that protein- and SMP-like molecules (i.e. regions I+II and IV) are the main compounds
273 retained by the submerged membrane. Conversely, humic-like substances (combining fulvic-
274 (III) and humic- (V) acid-like molecules) had the smallest rejection capacity due to their
275 lower molecular weight. No notable increase in total volume of fluorescence was observed in
276 the supernatant of the G-AnMBR over the time. Interestingly, Jacquin et al. (2017) concludes
277 that the protein-like regions are more associated with colloidal proteins whereas the SMP-like
278 are supposed to be macromolecular proteins present in the dissolved phase. These 3DEEM
279 fluorescence results support the substantial benefit of the membrane incorporation inside the
280 anaerobic reactor over the retention and bio-conversion of the macromolecules and colloids.
281 Instead of being taken away with the effluent, like in the UASB, these compounds are kept
282 into the supernatant and could be used as additional organic matter for biogas production.

283 **3.1.2 Suspended solids removal**

284 Concerning the suspended solids removal, nearly all suspended solids (SS) were
285 removed by the membrane filtration (Table 2). In comparison, an average of 10.8 mg/L was
286 found in the UASB effluent during the stable period which is much higher than the G-
287 AnMBR, even if it is under the 35 mgSS.L⁻¹ standard regulation discharge (Directive
288 91/271/EEC). Thus, the results emphasized that UASB combined with UF filtration for
289 DWWT at ambient temperature can achieve an excellent water quality (physical disinfection
290 and suspended matter retention).

291 **3.2 Biogas production**

292 Table 4 presents the results of methane quantification in the gas and the liquid phases.
293 Methane to carbon dioxide ratio of the biogas was around 80/20. This high methane content is
294 a benefit for the energy mass balance and shows a well-functioning of methanogens
295 populations (Chen et al., 2020). The methane flow rate achieved during the steady-state was

296 significantly upper in the G-AnMBR than in the UASB (0.85 ± 0.06 and 0.57 ± 0.05 NL-
297 $\text{CH}_4 \cdot \text{day}^{-1}$ respectively). Interestingly, only a slight difference was observed between methane
298 yields of 0.27 ± 0.03 for the G-AnMBR and 0.22 ± 0.04 $\text{L-CH}_4 \cdot \text{gCOD}_{\text{removed}}^{-1}$ for the UASB.
299 This result indicates that no significant improvement in sludge methanogenic activity was
300 observed with the incorporation of a membrane in spite of an increase in global carbon
301 conversion performances (Ozgun et al., 2015). It supports that membrane filtration enhances
302 the net production of methane by retaining particulate matter and DCOM (including VFA).
303 Longer contact time between organics and active biomass allows the conversion of slowly-
304 biodegradable matter and by-products into additional methane.

305 The concentration of methane inside the aqueous phase is about $12.8 \text{ mg-CH}_4 \cdot \text{L}^{-1}$ for the
306 G-AnMBR and $11.8 \text{ mg-CH}_4 \cdot \text{L}^{-1}$ in the UASB, which corresponds approximately to 22% and
307 27% respectively of the total methane produced. Some studies have demonstrated a saturation
308 degree lower in AnMBR than in UASB effluents (Gouveia et al., 2015a). This phenomenon is
309 mainly due to turbulences caused by membrane filtration operating conditions and fouling
310 mitigation technics used that provide a better mixing and so, a better gas-liquid transfer. In
311 this study, the results showed a saturation degree in the G-AnMBR of 2.00 ± 0.10 which is
312 slightly higher than the UASB where the value is 1.80 ± 0.07 . Saturation degrees obtained are
313 consistent with Smith et al. (2015) and Souza et al. (2011) results which found oversaturation
314 degrees about 2.2 at 15°C and 1.4-1.7 at 25°C respectively in a UASB treating domestic
315 wastewater. The closeness of the G-AnMBR and UASB values could be explained by the
316 same setup configurations and no fouling control method used aside intermittent filtration.
317 Therefore, no obvious hydrodynamic difference should occur between reactors.

318 By taking into consideration the whole methane generated ($C_{\text{CH}_4}^L + C_{\text{CH}_4}^G$), the methane
319 yields obtained were 0.33 ± 0.03 and 0.28 ± 0.04 $\text{NL-CH}_4 \cdot \text{gCOD}_{\text{removed}}^{-1}$ for the G-AnMBR
320 and UASB respectively. The closeness of the average methane yields measured to the

321 theoretical maximal value ($0.38 \text{ NL-CH}_4.\text{gCOD}_{\text{removed}}^{-1}$) demonstrates that an acclimatized
322 biomass could well-convert COD into methane at sub-optimal temperature. Methane yields
323 obtained in this study are in the high-range of the ones conventionally found in anaerobic
324 digestion studies that are mostly between $0.12\text{-}0.25 \text{ L-CH}_4.\text{gCOD}_{\text{removed}}^{-1}$. This high
325 conversion rate could be attributed to the long one-year acclimatization of the anaerobic
326 granular sludge at the operating conditions and to the relatively high VFA concentration in the
327 synthetic wastewater that promotes acetogenesis and methanogenesis pathways. Moreover, in
328 this study, the conversion rate takes into account the measured dissolved methane which is
329 generally neglected or estimated through Henry's law coefficient.

330 **3.3 COD mass balance**

331 COD mass balance for the G-AnMBR and UASB are presented in Fig. 3. It is apparent
332 from those results that the G-AnMBR allowed a higher removal rate of the COD since the
333 COD remaining in the UASB effluent is almost three-times higher. The total methane
334 produced by the anaerobic digestion process for the UASB and G-AMBR were 61.1% and
335 84.7% respectively but only 44.6% and 66.3% were in the gaseous phase and can be directly
336 valuable. This shows the importance to recover dissolved biogas from effluent to avoid
337 environmental issues but also to improve the potential energy recovery. These results are
338 consistent with those obtained by Ji et al. (2021) for an AnMBR pilot-scale treating raw
339 domestic wastewater with close operating conditions ($\text{OLR} = 0.72 \text{ kgCOD}.\text{m}^{-3}.\text{d}^{-1}$; $\text{HRT} =$
340 12h ; 25°C) where 10.7% of the COD was remaining in the effluent and 75% of the COD of
341 the influent was converted into methane of which 63% in gaseous phase. It can be seen that
342 the amounts of COD_{in} used for sulfate reduction and the one transformed into dissolved
343 biogas are nearly the same for both anaerobic reactors. This implies that the difference
344 between both methane conversion rate is due to the COD removal capacity and the use of
345 COD_{in} for biomass synthesis.

346 From the COD entering in the systems, 6.3% (G-AnMBR) and 14.7% (UASB) of the
347 COD were used for biomass production (Fig. 3). This suggests that a higher part of the COD_{in}
348 was consumed for biomass synthesis in the UASB and was therefore not available for
349 methane production. As a result, the calculated sludge yield was about 0.05
350 gVSS.gCOD_{removed}⁻¹ in the G-AnMBR against 0.11 gVSS.gCOD_{removed}⁻¹ in the UASB. The
351 sludge yield of the granular biomass corresponds to the typical low anaerobic sludge yield and
352 matches with previous AnMBR studies for DWWT at ambient temperature (see
353 supplementary material). The sludge yield in the UASB was twice higher than the one in the
354 G-AnMBR system. This phenomenon can be explained by the biomass washout occurring in
355 the UASB at the early stage because of the selective hydraulic pressure. According to the
356 Monod equation, the increase of the specific organic loading rate, caused by the loss of
357 flocculated sludge and small granules, stimulates the biomass growth (Chen et al., 2017;
358 Ozgun et al., 2015).

359 It should be noticed that in the case of AnMBR with external submerged membrane
360 configuration, the selective pressure is not overcome, though, there is an increase in the
361 biomass yield (Chen et al., 2017). Those findings suggest that the G-AnMBR configuration
362 with the membrane submerged inside the mixed granular anaerobic digester enhances the
363 conversion of the COD into methane while maintaining a low sludge production rate. This is
364 of great interest compared to conventional activated sludge processes since the energy
365 requirements as well as the treatment and disposal costs for sludge management could be
366 minimized.

367 **3.4 Granular sludge properties**

368 The settling ability and granulation behavior of the biomass were evaluated through the
369 SVI₃₀ and SVI₁₀ to SVI₃₀ ratio (see supplementary material). Both reactors were inoculated
370 with similar granular sludge SVI of 31.1 and 28.9 mL.gTS⁻¹ for UASB and G-AnMBR. Also,

371 the SVI_{10}/SVI_{30} ratio was around 1.3-1.4 meaning that the sludge is a mixture of readily
372 settleable granules and small granules and flocs with a lower capacity of settling. At the end
373 of the operation, SVI_{30} value for the UASB granular sludge decreased sharply (14.7 mL.gTS^{-1})
374 ¹⁾ and exhibited a SVI_{10}/SVI_{30} ratio of 1. These results confirm the selective pressure that
375 occurs in the UASB reactor where sole well-settleable granular biomass is kept into the
376 UASB. In contrast, the G-AnMBR configuration does not allow free and flocculated biomass
377 to run-off from the reactor and, as a result, higher SVI_{30} (22.9 mL.gTS^{-1}) and SVI_{10}/SVI_{30}
378 ratio (1.3) were measured in comparison to the UASB values.

379 Zeta potential was also measured as it gives an indication about the aptitude of sludge
380 biomass to aggregate among themselves. As suggested by others studies, a higher zeta
381 potential meaning a decline of the negative surface charge and, therefore, electrostatic
382 repulsion could be easily neutralized (Chen et al., 2017). Zeta potential values (see
383 supplementary material) were found higher at the end of the experiment than that at the
384 seeding for the G-AnMBR and UASB reactors suggesting that the biomass attachment has
385 been promoted during process operation.

386 Fig. 4 provides the changing in particle size distribution (PSD) of the granular sludge
387 for both reactors. Seed sludge for UASB and G-AnMBR showed almost identical profiles of
388 PSD corroborating the same inoculation. At the initial stage, large granules ($d_p \geq 0.63$)
389 accounted for $\approx 70\%$ of the total TS mass of the granular sludge whereas the main part of the
390 VS, commonly assimilated to active biomass, belonged to the medium fraction ($d_p 0.125-0.63$)
391 with $65 \pm 3 \%$ of the total VS mass. As expected, the flocs fraction represented a very low
392 amount of the total biomass since it has a small density compared to granular sludge. After
393 115 days of operation, a significant difference was observed for the granular sludge PSD of
394 the UASB reactor. As expected, shift to larger granules was observed in the UASB reactor
395 with 87.2% and 74.6% of the total TS and VS mass respectively measured in the biggest

396 fraction ($d_{p \geq 0.63}$). This hypothesizes that, besides the sludge washout of poor-settleable
397 particles, growth of larger-sized granules was promoted which is in accordance with the zeta
398 potential values. On the other hand, the granular sludge PSD of the G-AnMBR showed a
399 broader repartition because of the physical barrier retention that permitted the development of
400 various sludge type including free-bacteria and light flocs and granules. As reported in
401 previous studies, a wide variety of biomass (i.e. free-bacteria, fines flocs, granules, cake layer,
402 etc.) results in a large microbial diversity (Lin et al., 2011; Zhou et al., 2019). These results
403 clearly indicate that membrane incorporation enables to maintain the PSD tendency of the
404 granular sludge and leads to a more diversified anaerobic population by allowing the slow
405 growth of anaerobic methanogens (Lin et al., 2013). Moreover, frequent microbial samples
406 were taken during this experiment and will be later analyzed to characterize and confirm the
407 change in diversity and density of the microbial communities following the membrane
408 incorporation. Plus, further experiments should be conducted to evaluate the structural
409 stability of the granules with varying operating conditions to see the range of applicability of
410 the granular biomass.

411 VS/TS ratio depicts in Fig. 4 is an indicator to evaluate the amount of biomass within
412 the granular sludge. A global decrease in VS/TS ratio occurred in UASB intermediate and
413 smaller fractions while the decrease concerned particularly the intermediate granule fraction
414 in the G-AnMBR. This translates an increase in mineral content inside the granular fraction
415 that is exacerbated by biomass loss in the UASB. SEM-EDX analysis provided in
416 supplementary material indicates that the mineral part of the granular sludge was mainly
417 composed of calcium carbonate CaCO_3 . Prior studies stated that calcium concentration in
418 granules is negatively correlated to VS/TS ratio and bacterial specific activity. Core
419 calcification of granules is a harmful phenomenon as the calcium mineral precipitate and
420 calcium salts deposited in the outer layer limit the diffusion of molecules in granules

421 interstitial spaces (Zhang et al., 2021). It is likely that membrane attenuates the impact of
422 calcification by retaining the flocculated biomass within the reactor which further promote the
423 active biomass inside the granules (i.e. VS/TS ratio).

424 **3.5 G-AnMBR energy recovery evaluation and competitiveness**

425 Based on the methane produced from COD conversion, the energy potentially recovered
426 from DWWT was calculated. Table 5 provides an overview of net energy balance (NEB) and
427 effluent quality for the most common aerobic and anaerobic processes for DWWT at ambient
428 temperature. Anaerobic treatments have an evident energetic advantage comparing to the
429 aerobic DWWT that exhibits a negative NEB from -0.2 to -2 kWh.m⁻³. Although UASB has a
430 low energy demand and high energy recovery (NEB of 0.35-0.5 kWh.m⁻³), the effluent quality
431 obtained is not enough to meet discharge standards and to outcompete CAS or AeMBR
432 reactors (Chernicharo et al., 2015; Ozgun et al., 2013). Conversely, conventional AnMBR
433 reach high organics and suspended solids removal efficiencies but achieve a NEB close to
434 zero due to the gas-sparging energy-demand for membrane fouling control that accounts for
435 more than 70% of the process energy consumption (Smith et al., 2014). Therefore, it is
436 apparent from Table 5 that the G-AnMBR operated in this study is the only system which
437 allows both excellent effluent quality and strong positive net energy balance, even when the
438 dissolved methane is not recovered (0.58 kWh.m⁻³). This finding highlights the interest of the
439 G-AnMBR submerged configuration with no gas-sparging fouling control which optimizes at
440 the same time COD to methane conversion rate, energy-requirement, effluent quality and
441 reactor compactness. Hence, G-AnMBR technologies could be useful in poor-energy, water-
442 shortage and scarce-space areas (Kong et al., 2021a; Robles et al., 2018). In addition,
443 considering the complete recovery of dissolved biogas, nearly 0.20 kWh.m⁻³ of additional
444 energy could be generated from the domestic WW by G-AnMBR treatment. As mentioned
445 above, it points out that the dissolved methane recovery needs further investigation as it

446 accounts for more than 25% of the total produced methane and because methane is an
447 important greenhouse concern (Gouveia et al., 2015; Ji et al., 2021; Smith et al., 2013).

448 **Conclusion**

449 It has been demonstrated that the submerged G-AnMBR configuration, without gas
450 sparging, represents a sustainable biotechnology for DWWT at ambient temperatures over
451 conventional processes with regard to effluent quality and energy requirements. The
452 membrane barrier helped to maintain the process stability, led to a broader sludge diversity
453 with no granular sludge activity alteration. The G-AnMBR reached organic removal rate as
454 high as aerobic process with a tCOD removal of ~92.3%. The NEB was maximized to +0.58
455 kWh.m⁻³ with the G-AnMBR setup without gas-sparging, bringing the G-AnMBR as a
456 promising process which may be part of the circular economy strategies.

457 **Acknowledgments**

458 This work was supported by a grant overseen by the French National Research Agency
459 as part of the “JCJC” Program BàMAn (ANR-18-CE04-0001-01). Special thanks are
460 addressed to Patrice Montels and Daniel Valenza (IEM) for the pilot design and building and
461 Didier Cot and Bertrand Rebière (IEM) for the SEM-EDX analysis.

462 **References**

463 APHA, AWWA, WEF (Eds.), 1998. Standard methods: for the examination of water and
464 wastewater, 20. ed. ed. American Public Health Association, Washington, DC.

465 Batstone, D.J., Viridis, B., 2014. The role of anaerobic digestion in the emerging energy
466 economy. *Current Opinion in Biotechnology, Energy biotechnology • Environmental*
467 *biotechnology* 27, 142–149.

468 Chen, C., Guo, W., Ngo, H.H., 2016. Advances in Granular Growth Anaerobic
469 Membrane Bioreactor (G-AnMBR) for Low Strength Wastewater Treatment 7.

470 Chen, C., Guo, W., Ngo, H.H., Chang, S.W., Duc Nguyen, D., Dan Nguyen, P., Bui,
471 X.T., Wu, Y., 2017. Impact of reactor configurations on the performance of a granular
472 anaerobic membrane bioreactor for municipal wastewater treatment. *International*
473 *Biodeterioration & Biodegradation* 121, 131–138.

474 Chen, C., Liu, Z., Huang, X., 2020. 14 - Anaerobic membrane bioreactors for sustainable
475 and energy-efficient municipal wastewater treatment, in: Ngo, H.H., Guo, W., Ng, H.Y.,
476 Mannina, G., Pandey, A. (Eds.), *Current Developments in Biotechnology and Bioengineering*.
477 Elsevier, pp. 335–366.

478 Chen, R., Nie, Y., Ji, J., Utashiro, T., Li, Q., Komori, D., Li, Y., 2017. Submerged
479 anaerobic membrane bioreactor (SAnMBR) performance on sewage treatment: removal
480 efficiencies, biogas production and membrane fouling. *Water science and technology* 76,
481 1308–1317.

482 Chernicharo, C.A.L., van Lier, J.B., Noyola, A., Bressani Ribeiro, T., 2015. Anaerobic
483 sewage treatment: state of the art, constraints and challenges. *Rev Environ Sci Biotechnol* 14,
484 649–679.

485 Deng, L., Guo, W., Ngo, H.H., Zhang, J., Liang, S., 2020. Advanced anaerobic
486 membrane bioreactors: Performance enhancers and their hybrid systems, in: Ngo, H.H., Guo,
487 W., Ng, H.Y., Mannina, G., Pandey, A. (Eds.), *Current Developments in Biotechnology and*
488 *Bioengineering*. Elsevier, pp. 109–142.

489 Derlon, N., Wagner, J., da Costa, R.H.R., Morgenroth, E., 2016. Formation of aerobic
490 granules for the treatment of real and low-strength municipal wastewater using a sequencing
491 batch reactor operated at constant volume. *Water Research* 105, 341–350.

492 Giménez, J.B., Martí, N., Ferrer, J., Seco, A., 2012. Methane recovery efficiency in a
493 submerged anaerobic membrane bioreactor (SAnMBR) treating sulphate-rich urban
494 wastewater: Evaluation of methane losses with the effluent. *Bioresource Technology* 118, 67–
495 72.

496 Gouveia, J., Plaza, F., Garralon, G., Fdz-Polanco, F., Peña, M., 2015. A novel
497 configuration for an anaerobic submerged membrane bioreactor (AnSMBR). Long-term
498 treatment of municipal wastewater under psychrophilic conditions. *Bioresource Technology*
499 198, 510–519.

500 Iorhemen, O.T., Hamza, R.A., Tay, J.H., 2017. Membrane fouling control in membrane
501 bioreactors (MBRs) using granular materials. *Bioresource Technology*, Special issue on
502 Challenges in Environmental Science and Engineering, CESE-2016 240, 9–24.

503 Jacquin, C., Lesage, G., Traber, J., Pronk, W., Heran, M., 2017. Three-dimensional
504 excitation and emission matrix fluorescence (3DEEM) for quick and pseudo-quantitative
505 determination of protein- and humic-like substances in full-scale membrane bioreactor
506 (MBR). *Water Res* 118, 82–92.

507 Ji, J., Ni, J., Ohtsu, A., Isozumi, N., Hu, Y., Du, R., Chen, Y., Qin, Y., Kubota, K., Li, Y.-
508 Y., 2021. Important effects of temperature on treating real municipal wastewater by a
509 submerged anaerobic membrane bioreactor: Removal efficiency, biogas, and microbial
510 community. *Bioresour Technol* 336, 125306.

511 Jones, E.R., van Vliet, M.T.H., Qadir, M., Bierkens, M.F.P., 2021. Country-level and
512 gridded estimates of wastewater production, collection, treatment and reuse. *Earth System*
513 *Science Data* 13, 237–254.

514 Kong, Z., Li, L., Wu, J., Wang, T., Rong, C., Luo, Z., Pan, Y., Li, D., Li, Y., Huang, Y.,
515 Li, Y.-Y., 2021a. Evaluation of bio-energy recovery from the anaerobic treatment of
516 municipal wastewater by a pilot-scale submerged anaerobic membrane bioreactor (AnMBR)
517 at ambient temperature. *Bioresource Technology* 339, 125551.

518 Kong, Z., Wu, J., Rong, C., Wang, T., Li, L., Luo, Z., Ji, J., Hanaoka, T., Sakemi, S., Ito,
519 M., Kobayashi, S., Kobayashi, M., Qin, Y., Li, Y.-Y., 2021b. Large pilot-scale submerged
520 anaerobic membrane bioreactor for the treatment of municipal wastewater and biogas
521 production at 25 °C. *Bioresour Technol* 319, 124123.

522 Layer, M., Adler, A., Reynaert, E., Hernandez, A., Pagni, M., Morgenroth, E., Holliger,
523 C., Derlon, N., 2019. Organic substrate diffusibility governs microbial community
524 composition, nutrient removal performance and kinetics of granulation of aerobic granular
525 sludge. *Water Research X* 4, 100033.

526 Liao, B.-Q., Kraemer, J.T., Bagley, D.M., 2006. Anaerobic Membrane Bioreactors:
527 Applications and Research Directions. *Critical Reviews in Environmental Science and*
528 *Technology* 36, 489–530.

529 Lin, H., Peng, W., Zhang, M., Chen, J., Hong, H., Zhang, Y., 2013. A review on
530 anaerobic membrane bioreactors: Applications, membrane fouling and future perspectives.
531 *Desalination* 314, 169–188.

532 Lin, H.J., Gao, W.J., Leung, K.T., Liao, B.Q., 2011. Characteristics of different fractions
533 of microbial flocs and their role in membrane fouling. H. J. Lin et al. Characteristics of different
534 fractions of microbial flocs in membrane fouling. *Water Sci Technol* 63, 262–269.

535 Lobato, L.C.S., Chernicharo, C.A.L., Souza, C.L., 2012. Estimates of methane loss and
536 energy recovery potential in anaerobic reactors treating domestic wastewater. *Water Science
537 and Technology* 66, 2745–2753.

538 Maaz, M., Yasin, M., Aslam, M., Kumar, G., Atabani, A.E., Idrees, M., Anjum, F., Jamil,
539 F., Ahmad, R., Khan, A.L., Lesage, G., Heran, M., Kim, J., 2019. Anaerobic membrane
540 bioreactors for wastewater treatment: Novel configurations, fouling control and energy
541 considerations. *Bioresource Technology* 283, 358–372.

542 Ozgun, H., Dereli, R.K., Ersahin, M.E., Kinaci, C., Spanjers, H., van Lier, J.B., 2013. A
543 review of anaerobic membrane bioreactors for municipal wastewater treatment: Integration
544 options, limitations and expectations. *Separation and Purification Technology* 118, 89–104.

545 Ozgun, H., Gimenez, J.B., Ersahin, M.E., Tao, Y., Spanjers, H., van Lier, J.B., 2015.
546 Impact of membrane addition for effluent extraction on the performance and sludge
547 characteristics of upflow anaerobic sludge blanket reactors treating municipal wastewater.
548 *Journal of Membrane Science* 479, 95–104.

549 Robles, Á., Ruano, M.V., Charfi, A., Lesage, G., Heran, M., Harmand, J., Seco, A.,
550 Steyer, J.-P., Batstone, D.J., Kim, J., Ferrer, J., 2018. A review on anaerobic membrane
551 bioreactors (AnMBRs) focused on modelling and control aspects. *Bioresource Technology*
552 270, 612–626.

553 Rocco, P., Vagliasindi, F.G.A., 2020. Membrane bioreactors for wastewater
554 reclamation: Cost analysis, in: *Current Developments in Biotechnology and Bioengineering*.
555 Elsevier, pp. 311–322.

556 Safitri, A.S., Hamelin, J., Kommedal, R., Milferstedt, K., 2021. Engineered
557 methanotrophic syntrophy in photogranule communities removes dissolved methane. *Water*
558 *Research X* 12, 100106.

559 Smith, A.L., J. Skerlos, S., Raskin, L., 2015. Anaerobic membrane bioreactor treatment
560 of domestic wastewater at psychrophilic temperatures ranging from 15 °C to 3 °C.
561 *Environmental Science: Water Research & Technology* 1, 56–64.

562 Smith, A.L., Skerlos, S.J., Raskin, L., 2013. Psychrophilic anaerobic membrane
563 bioreactor treatment of domestic wastewater. *Water Research* 47, 1655–1665.

564 Smith, A.L., Stadler, L.B., Cao, L., Love, N.G., Raskin, L., Skerlos, S.J., 2014.
565 *Navigating Wastewater Energy Recovery Strategies: A Life Cycle Comparison of Anaerobic*
566 *Membrane Bioreactor and Conventional Treatment Systems with Anaerobic Digestion*.
567 *Environ. Sci. Technol.* 48, 5972–5981.

568 Sohaib, Q., Kalakech, C., Charmette, C., Cartier, J., Lesage, G., Mericq, J.-P., 2022.
569 *Hollow-Fiber Membrane Contactor for Biogas Recovery from Real Anaerobic Membrane*
570 *Bioreactor Permeate*. *Membranes* 12, 112.

571 Souza, C.L., Chernicharo, C.A.L., Aquino, S.F., 2011. Quantification of dissolved
572 methane in UASB reactors treating domestic wastewater under different operating conditions.
573 *Water Sci Technol* 64, 2259–2264.

574 Srinivasa Raghavan, D.S., Qiu, G., Song, Y., Ting, Y.-P., 2017. Anaerobic Treatment of
575 Low-Strength Wastewater, in: *Current Developments in Biotechnology and Bioengineering*.
576 Elsevier, pp. 293–320.

577 Su, X., Chiang, P., Pan, S., Chen, G., Tao, Y., Wu, G., Wang, F., Cao, W., 2019.
578 Systematic approach to evaluating environmental and ecological technologies for wastewater
579 treatment. *Chemosphere* 218, 778–792.

580 van Lier, J.B., Mahmoud, N., Zeeman, G., 2008. *Anaerobic Wastewater Treatment*, in:
581 *Biological Wastewater Treatment: Principles, Modelling and Design*. IWA Publishing.

582 Vinardell, S., Astals, S., Peces, M., Cardete, M.A., Fernández, I., Mata-Alvarez, J.,
583 Dosta, J., 2020. Advances in anaerobic membrane bioreactor technology for municipal
584 wastewater treatment: A 2020 updated review. *Renewable and Sustainable Energy Reviews*
585 130, 109936.

586 Zhang, J., Pan, J.-Q., Zhao, S., Gan, P., Qin, C.-R., Wang, Z.-W., Chen, Y., Liu, X., Lu,
587 L.-H., Wang, S.-F., 2021. Calcium migration inside anaerobic granular sludge: Evidence from
588 calcium carbonate precipitation pattern. *Colloids and Surfaces A: Physicochemical and*
589 *Engineering Aspects* 625, 126890.

590 Zhou, Z., Tao, Y., Zhang, S., Xiao, Y., Meng, F., Stuckey, D.C., 2019. Size-dependent
591 microbial diversity of sub-visible particles in a submerged anaerobic membrane bioreactor
592 (SAnMBR): Implications for membrane fouling. *Water Research* 159, 20–29.

593 Table 1 - G-AnMBR and UASB operating conditions (mean values \pm SD).

Parameter	G-AnMBR	UASB
Temperature ($^{\circ}$ C)	25.0 ± 0.8	25.8 ± 1.8
pH (-)	7.0 ± 0.2	7.1 ± 0.2
Redox (mV)	-462 ± 37	-456 ± 32
Jp _{20,NET} (LMH)	1.34 ± 0.14	-
Jp _{20,INST}	2.48 ± 0.22	-
HRT (h)	13.1 ± 2.0	13.2 ± 3.0
OLR (kgCOD.m ⁻³ .d ⁻¹)	0.50 ± 0.14	0.48 ± 0.15
ULV (m.h ⁻¹)	2.25	2.04

594

595 Table 2 - Effluent composition and removal efficiencies of the G-AnMBR and UASB (mean values \pm SD ;
 596 $n \geq 20$).

Phase		G-AnMBR permeate		UASB effluent	
		Transient	Steady	Transient	Steady
tCOD _{eff}	(mg/L)	43.3 \pm 13.1	22.0 \pm 14.5	150.2 \pm 36.0	59.0 \pm 28.5
tCOD _{removal}	(%)	81.6 \pm 3.8	92.3 \pm 4.1	35.9 \pm 12.6	79.2 \pm 8.5
sCOD _{eff}	(mg/L)	43.3 \pm 13.1	22.0 \pm 14.5	69.0 \pm 8.1	44.1 \pm 18.9
sCOD _{removal}	(%)	76.7 \pm 3.6	90.0 \pm 5.4	63.9 \pm 7.8	80.7 \pm 7.3
DOC _{eff}	(mg/L)	7.5 \pm 0.0	2.1 \pm 0.6	23.6 \pm 0.0	13.8 \pm 9.4
DOC _{removal}	(%)	85.7 \pm 0.0	97.8 \pm 1.0	60.0 \pm 0.0	86.5 \pm 9.1
MLSS _{eff}	(mg/L)	ND	ND	113.1 \pm 87.7	10.8 \pm 6.0
MLVSS _{eff}	(mg/L)	ND	ND	60.4 \pm 37.4	9.3 \pm 5.4

597 ND : non-detectable

598

599 Table 3 - Average normalized volume of fluorescence for the different regions of the 3DEEM spectra for G-
 600 AnMBR supernatant and permeate and UASB effluent and the membrane rejection during the steady-state
 601 period. Errors represent standard deviation (n=7).

		3DEEM Region			
		I+II	IV	III+V	Total
G-AnMBR	Supernatant ($\times 10^8$ A.U/nm ²)	2.74 \pm 1.04	0.12 \pm 0.03	0.52 \pm 0.09	3.38 \pm 1.10
	Permeate ($\times 10^8$ A.U/nm ²)	1.46 \pm 0.68	0.05 \pm 0.01	0.40 \pm 0.07	1.90 \pm 0.69
	Membrane rejection (%)	45.9 \pm 20.0	59.8 \pm 18.3	24.0 \pm 14.6	42.3 \pm 17.6
UASB	Effluent ($\times 10^8$ A.U/nm ²)	2.45 \pm 1.40	0.12 \pm 0.08	0.45 \pm 0.14	3.02 \pm 1.59

602

603 Table 4 - Methane production in the gas phase and liquid phase (mean values \pm SD ; n \geq 15).

	Unit	G-AnMBR	UASB
CH ₄ flow rate	NL-CH ₄ .day ⁻¹	0.85 \pm 0.06	0.57 \pm 0.05
CH ₄ /CO ₂ ratio	% / %	79.9/20.1 \pm 3.5	81.9/18.1 \pm 6.8
Gaseous methane yield	NL-CH ₄ /g-COD _{removed}	0.27 \pm 0.03	0.22 \pm 0.04
Dissolved methane	mg-CH ₄ .L ⁻¹	12.8 \pm 0.7	11.7 \pm 1.1
Degree of saturation	-	2.00 \pm 0.10	1.80 \pm 0.07
Dissolved CH ₄ flow rate	NL-CH ₄ .day ⁻¹	0.24 \pm 0.01	0.22 \pm 0.02
Total methane yield	NL-CH ₄ /g-COD _{removed}	0.33 \pm 0.03	0.28 \pm 0.04

604

605 Table 5 - Comparison of net energy balance and effluent quality between aerobic and anaerobic technologies for
 606 low-strenght domestic wastewater treatment at ambient temperature ($\leq 25^{\circ}\text{C}$).

	Energy consumption (kWh.m^{-3})	Energy from CH_4 (kWh.m^{-3})	Net Energy Balance (kWh.m^{-3})	Effluent quality	
				COD removal (%)	Effluent TSS (mg.L^{-1})
CAS	0.2 – 0.8 ^{a,b}	-	-0.2 – -0.8	85-93 ^a	<30
AeMBR	0.6 – 2 ^{b,c}	-	-0.6 – -2	>95 ^a	<1 ^c
UASB	0.11 ^d	0.6 ^d	0.5	40-80 ^{g,h}	60-200 ^h
		0.46 (0.64*) ^j	0.35 (0.53*)	79 ^j	$\cong 10$ ^j
AnMBR	0.3 – 0.5 ^{e,f}	0.3 – 0.4 ^{e,f}	-0.1 – 0.1	>80-90 ⁱ	<1 ^{h,i}
G-AnMBR	0.12 ^j	0.70 (0.89*) ^j	0.58 (0.77*)	92 ^j	<1 ^j
				>90 ⁱ	

607 a. (Su et al., 2019) ; b. (Roccaro and Vagliasindi, 2020) ; c. (Liao et al., 2006) ; d. (Lobato. Chernicharo. et
 608 Souza 2012) ; e. (Kong et al., 2021a) ; f. (Smith et al., 2014) ; g. (van Lier et al., 2008) ; h. (Chernicharo et al.,
 609 2015) ; i. (Chen et al., 2020) ; j. This study.

610 (_*) Those values in brackets take into account the complete dissolved methane recovery.
 611 MBR values are for submerged membrane configuration.

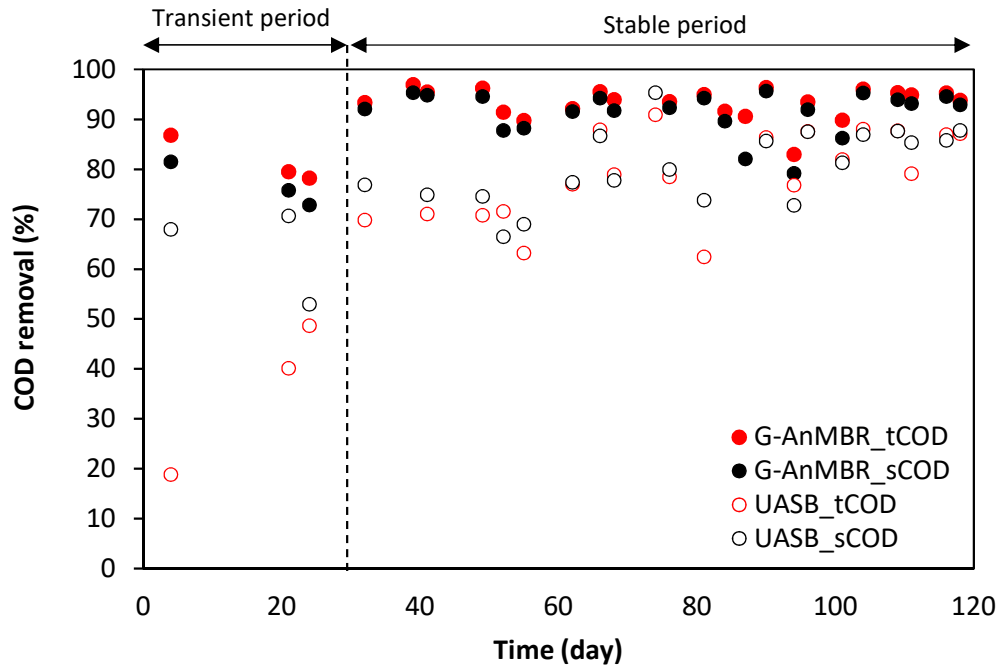


Fig. 1 - Total and soluble COD removal efficiencies in the UASB effluent and AnMBR permeate during the 120 days of operation.

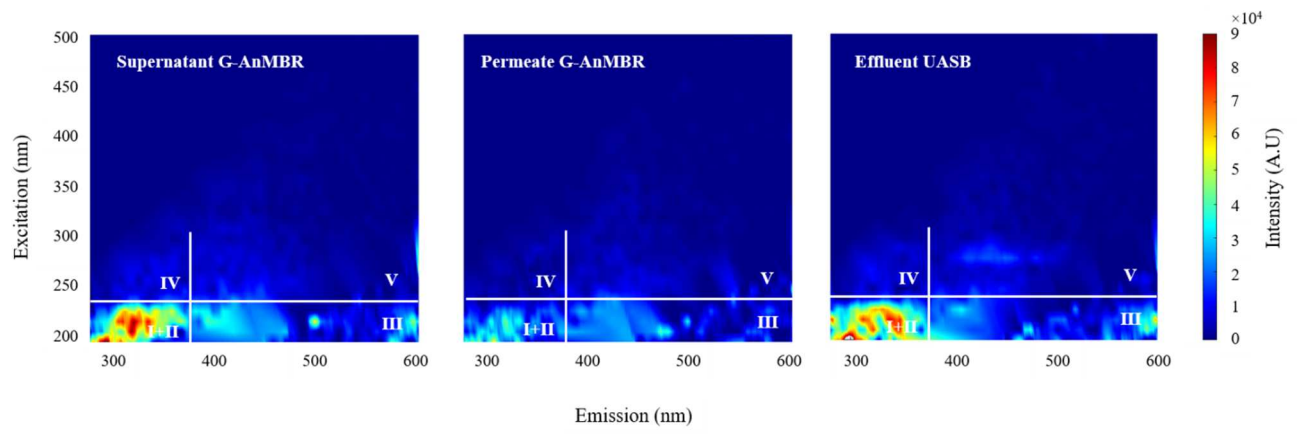


Fig. 2 - 3DEEM fluorescence spectra of G-AnMBR supernatant and permeate and UASB effluent on day 94

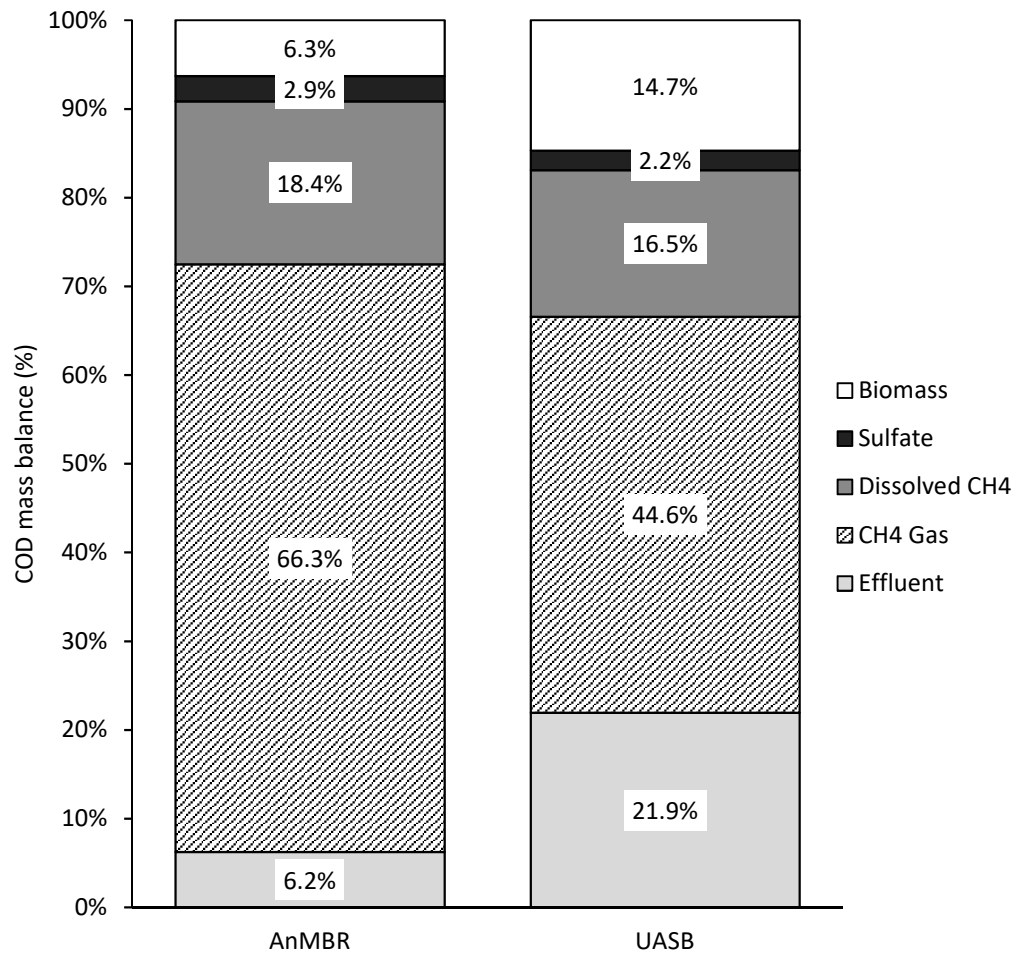
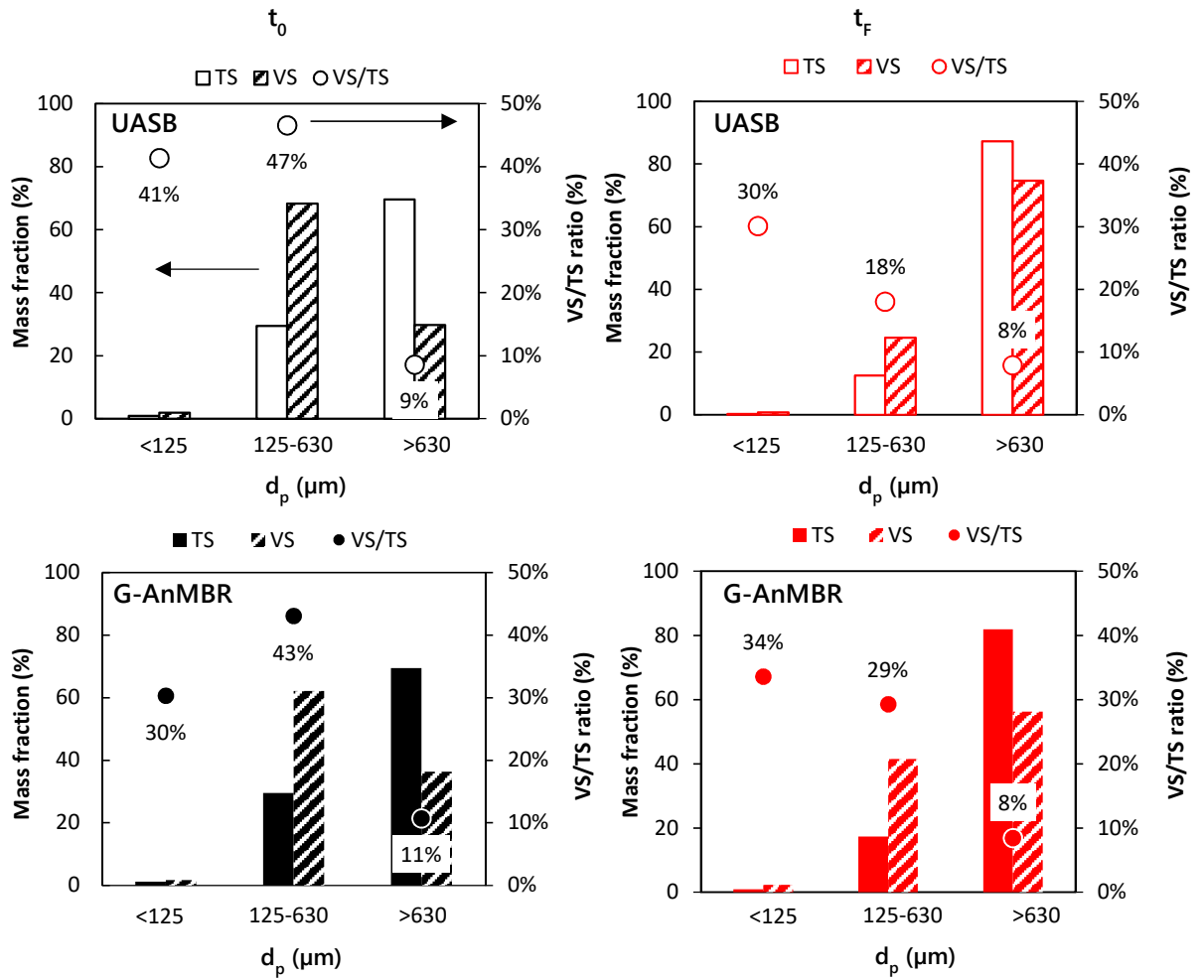


Fig. 3 - Average COD mass balance in the UASB and G-AnMBR reactors during the steady-state period (from day 30 to 120).



1

2 Fig. 4- Particle size distribution of the UASB and G-AnMBR granular sludge at the beginning (t₀ = day 1)
 3 and at the end (t_F = day 115) of the experiment.

